computation

MDPI

Article

Application of DFT and TD-DFT on Langmuir Adsorption of Nitrogen and Sulfur Heterocycle Dopants on an Aluminum Surface Decorated with Magnesium and Silicon

Fatemeh Mollaamin [1,2,*] and Majid Monajjemi [3]

[1] Department of Food Engineering, Faculty of Engineering and Architecture, Kastamonu University, 37150 Kastamonu, Turkey
[2] Department of Biology, Faculty of Science, Kastamonu University, 37150 Kastamonu, Turkey
[3] Department of Chemical Engineering, Central Tehran Branch, Islamic Azad University, Tehran 1496969191, Iran; maj.monajjemi@iauctb.ac.ir
* Correspondence: smollaamin@gmail.com

Abstract: In this study, we investigated the abilities of nitrogen and sulfur heterocyclic carbenes of benzotriazole, 2-mercaptobenzothiazole, 8-hydroxyquinoline, and 3-amino-1,2,4-triazole-5-thiol regarding adsorption on an Al-Mg-Si alloy toward corrosion inhibition of the surface. Al-Si(14), Al-Si(19), and Al-Si(21) in the Al-Mg-Si alloy surface with the highest fluctuation in the shielding tensors of the "NMR" spectrum generated by intra-atomic interaction directed us to the most influence in the neighbor atoms generated by interatomic reactions of N → Al, O → Al, and S → Al through the coating and adsorbing process of Langmuir adsorption. The values of various thermodynamic properties and dipole moments of benzotriazole, 2-mercaptobenzothiazole, 8-hydroxyquinoline, and 3-amino-1,2,4-triazole-5-thiol adsorbed on the Al-Mg-Si increased by enhancing the molecular weight of these compounds as well as the charge distribution between organic compounds (electron donor) and the alloy surface (electron acceptor). Finally, this research can build up our knowledge of the electronic structure, relative stability, and surface bonding of various metal alloy surfaces, metal-doped alloy nanosheets, and other dependent mechanisms such as heterogeneous catalysis, friction lubrication, and biological systems.

Keywords: Langmuir adsorption; benzotriazole; 2-mercaptobenzothiazole; 8-hydroxyquinoline; 3-amino-1,2,4-triazole-5-thiol; Al-Mg-Si; ONIOM; CAM-DFT; NMR; NBO; IR; UV–vis; HOMO; LUMO

Citation: Mollaamin, F.; Monajjemi, M. Application of DFT and TD-DFT on Langmuir Adsorption of Nitrogen and Sulfur Heterocycle Dopants on an Aluminum Surface Decorated with Magnesium and Silicon. *Computation* **2023**, *11*, 108. https://doi.org/10.3390/computation11060108

Academic Editor: Aleksey E. Kuznetsov

Received: 24 March 2023
Revised: 16 May 2023
Accepted: 18 May 2023
Published: 29 May 2023

1. Introduction

Among the various methods that minimize corrosion of metal surfaces, its inhibition by organic molecules is one of the most applicable methods because of its stability and low cost [1–12]. The existence of multiple bonds with π-electrons in these inhibitors help extensively in the formation of inactive blocks on metal surface and alloys, thereby closing the active sites of corrosion [13–22].

Based on some research, benzotriazole, 2-mercaptobenzothiazole, 8-hydroxyquinoline, and 3-amino-1,2,4-triazole-5-thiol are organic cyclic inhibitors for metal, semi-metal, or non-metal surfaces and their alloys by preventing undesirable surface reactions. It is obvious that a passive layer containing a complex between the surface and these inhibitors is generated when the surface is immersed in a solution consisting of benzotriazole, 2-mercaptobenzothiazole, 8-hydroxyquinoline, and 3-amino-1,2,4-triazole-5-thiol. The passive layer is insoluble in aqueous and many organic solutions. There is a positive connection between the thickness of the passive layer and the efficiency of preventing corrosion [23–26].

In the present work, we investigated adding some alloying elements of magnesium and silicon to an aluminum surface to form A-Mg-Si complex that was coated with organic

compounds of benzotriazole, 2-mercaptobenzothiazole, 8-hydroxyquinoline, and 3-amino-1,2,4-triazole-5-thiol as the corrosion inhibitors of Al-Mg-Si alloy surface.

2. Theory, Materials, and Method

2.1. Heterocycle Inhibiting Agents

Recently, some researchers investigated how organic compounds can be employed as corrosion inhibitors for Al and its alloys because they consist of several heteroatoms (nitrogen, sulfur, oxygen, and phosphorus) that act as active adsorption centers. In this paper, we discuss the use of organic compounds of benzotriazole, 2-mercaptobenzothiazole, 8-hydroxyquinoline, and 3-amino-1,2,4-triazole-5-thiol as the corrosion inhibitors of an Al-Mg-Si alloy surface [27,28].

In this work, it was attributed to the inhibiting influence of the benzotriazole, 2-mercaptobenzothiazole, 8-hydroxyquinoline, and 3-amino-1,2,4-triazole-5-thiol on the adsorption of a stable complex on the aluminum alloy of the Al-Mg-Si surface.

2.2. Langmuir Adsorption Theory

The adsorption of benzotriazole, 2-mercaptobenzothiazole, 8-hydroxyquinoline, and 3-amino-1,2,4-triazole-5-thiol as corrosion inhibitors on the aluminum alloy surface of Al-Mg-Si in NaCl solution was performed [29–31] (Scheme 1).

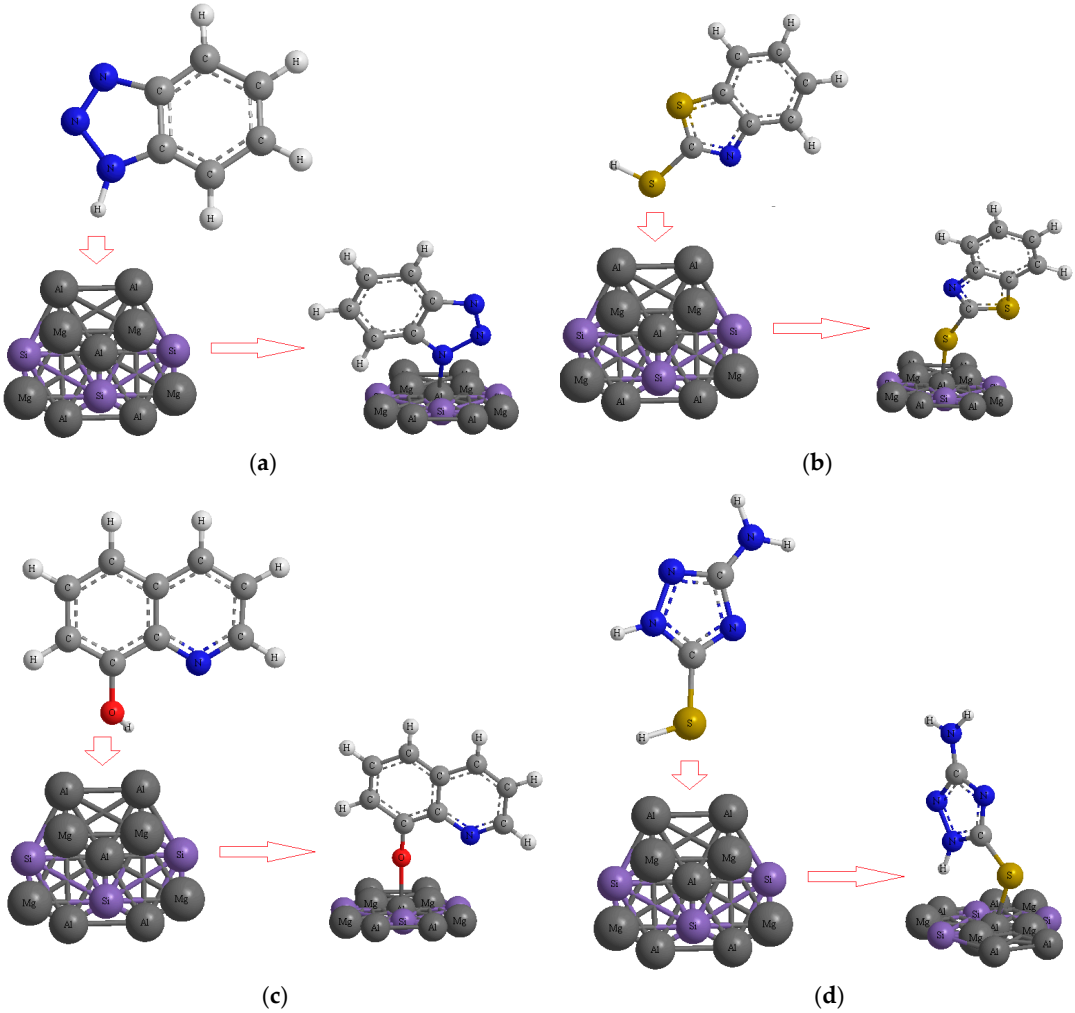

Scheme 1. Mechanism of Langmuir adsorption of the organic corrosion inhibitors of (**a**) benzotriazole, (**b**) 2-mercaptobenzothiazole, (**c**) 8-hydroxyquinoline, and (**d**) 3-amino-1,2,4-triazole-5-thiol on an Al-Mg-Si alloy surface.

2.3. Conceptual "ONOIM"

The three-layered pattern was applied for effective barriers of benzotriazole, 2-mercaptobenzothiazole, 8-hydroxyquinoline, and 3-amino-1,2,4-triazole-5-thiol adsorbing on an Al-Mg-Si alloy surface (Scheme 2) [32,33].

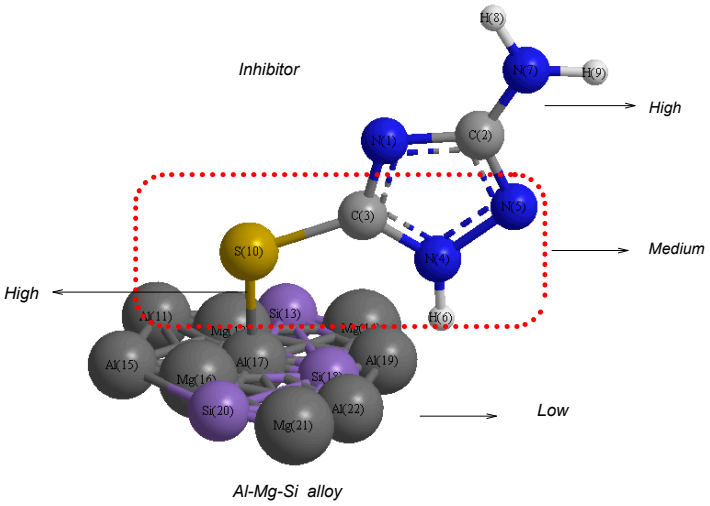

Scheme 2. The "ONIOM" layer of adsorption mechanism of N-heterocyclic carbene on an Al-Mg-Si alloy surface based on optimized coordination.

We found that the surface binding site preferences of the N-atom of benzotriazole, O-atom of 8-hydroxyquinoline, and S-atom of both 2-mercaptobenzothiazole and 3-amino-1,2,4-triazole-5-thiol on the adsorption site were largely affected by the presence of neighboring atoms (Scheme 2).

The average composition and crystal lattice parameters of Al-Mg-Si with a needle shape were considered based on Miller indices (including a = 6.75, b = 4.05, and c = 7.94 Å) [34–36].

The resulting observations showed that the Al-Mg-Si alloy surface calculated with the obtained structure properties was in good agreement with those metal alloys from other experimental computations [37–42].

2.4. DFT Calculations

The Al-Mg-Si alloy surface was built with a rigid system and a "Z-Matrix" format, for which a blank line was placed and after that, the following information has been illustrated. The rigid "PES" was performed with the "CAM-B3LYP" functional [43–49] while employing the "6-31+ G (d,p)/EPRIII/LANL2DZ" basis sets [50] for benzotriazole, 8-hydroxyquinoline, 2-mercaptobenzothiazole, and 3-amino-1,2,4-triazole-5-thiol adsorbing onto the Al-Mg-Si alloy surface using the "Gaussian 16" program package [35]. For the Al alloy surface, the small energy difference between the formations of adsorbate → Al-Mg-Si alloy complex could direct us to a somewhat coated surface for preventing the corrosion.

3. Results and Discussion

Many inhibitors reduce or prohibit the corrosion of aluminum via either cathode or anodic reactions. Usage of chromates (which extinguish the anodic reactions with coatings as the inhibitions for aluminum sheets) has been reduced because of toxicity. Other compounds such as phosphates, silicates, nitrates, nitrites, benzoates, and N-heterocyclic structures can influence the cathodic reactions in an aqueous environment.

In this study, the susceptibility of organic inhibitors (benzotriazole, 2-mercapto benzothiazole, 8-hydroxyquinoline, and 3-amino-1,2,4-triazole-5-thiol), the characteristics of the aluminum alloy surface (Al-Mg-Si), and the adsorption conditions were considerable.

3.1. Infrared Spectroscopy Analysis

The infrared specifications around 1500–3500 cm^{-1} for benzotriazole → Al-Mg-Si, 2-mercaptobenzothiazole → Al-Mg-Si, 8-hydroxyquinoline → Al-Mg-Si, and 3-amino-1,2,4-triazole-5-thiol → Al-Mg-Si with the strongest peak at approximately 2700–2750 cm^{-1} are reported in Figure 1a–d.

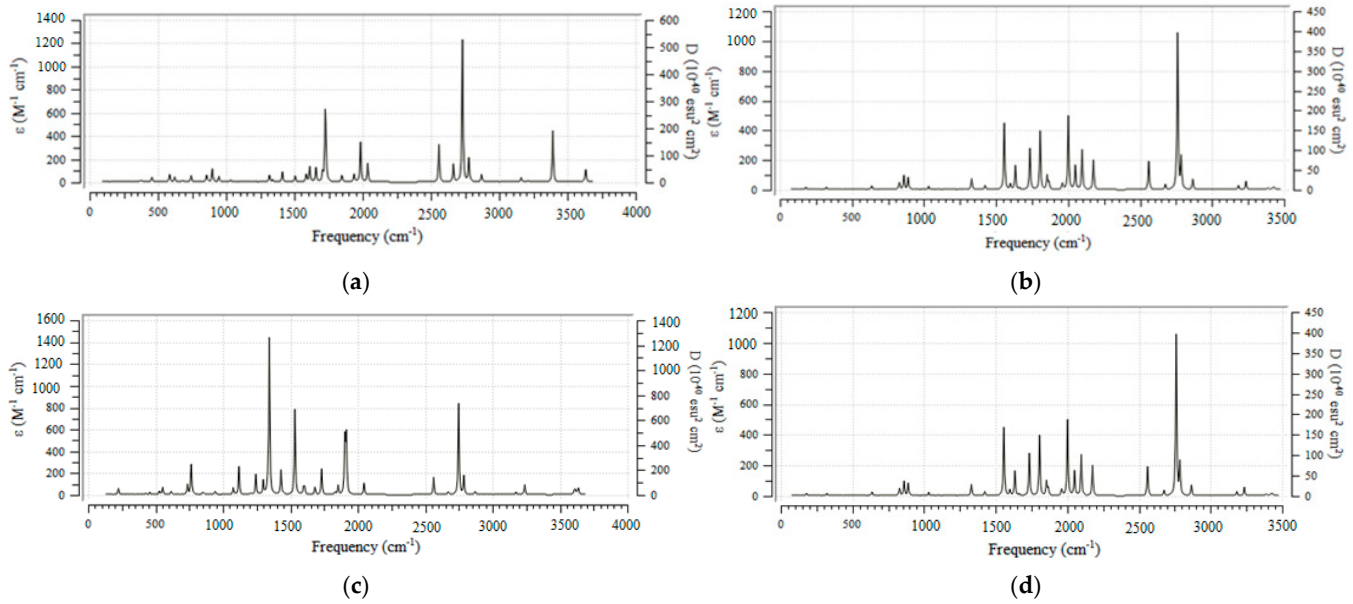

Figure 1. Infrared specifications for (**a**) benzotriazole → Al-Mg-Si, (**b**) 2-mercaptobenzothiazole → Al-Mg-Si, (**c**) 8-hydroxyquinoline → Al-Mg-Si, and (**d**) 3-amino-1,2,4-triazole-5-thiol → Al-Mg-Si using the "CAM-B3LYP" method with "6-31+ G (d,p)/EPRIII/LANL2DZ" basis sets. ε ($M^{-1}cm^{-1}$ or $Lmol^{-1}cm^{-1}$) is the absorbance unit and D (10^{-4} esu^2 cm^2) is the dipole strength via the esu or electrostatic unit, which is *a unit of charge in the cgs (centimeter-gram-second) system*.

The vibrational calculations were done for an aluminum alloy of Al-Mg-Si interacting with four organic inhibitors including benzotriazole, 2-mercaptobenzothiazole, 8-hydroxyquinoline, and 3-amino-1,2,4-triazole-5-thiol adsorbed onto this alloy surface, which produced the complexes of benzotriazole → Al-Mg-Si, 2-mercaptobenzothiazole → Al-Mg-Si, 8-hydroxyquinoline → Al-Mg-Si, and 3-amino-1,2,4-triazole-5-thiol → Al-Mg-Si (Table 1).

Table 1. Thermochemical traits for benzotriazole, 2-mercaptobenzothiazole, 8-hydroxyquinoline, and 3-amino-1,2,4-triazole-5-thiol as corrosion inhibitors on the aluminum alloy surface of Al-Mg-Si in NaCl solution at 300 K.

Compound	ΔH° × 10^{-4} (kcal/mol)	ΔG° × 10^{-4} (kcal/mol)	S° (cal/K·mol)	Dipole Moment (Debye)
Al-Mg-Si	−177.5928	−177.5950	75.321	1.7232
Benzotriazole	−24.5172	−24.5196	80.255	3.3166
Benzotriazole →Al-Mg-Si	−202.0579	−202.0606	88.085	5.7312
2-Mercaptobenzothiazole	−69.5234	−69.5260	85.643	2.5108
2-Mercaptobenzothiazole → Al-Mg-Si	−247.0475	−247.0503	92.232	3.3983
8-Hydroxyquinoline	−29.5526	−29.5551	83.336	1.6389
8-Hydroxyquinoline → Al-Mg-Si	−207.1047	−207.1074	91.009	2.7204
3-Amino-1,2,4-triazole-5-thiol	−43.1336	−43.1358	73.839	1.5672
3-Amino-1,2,4-triazole-5-thiol → Al-Mg-Si	−220.6678	−220.6704	87.657	2.4627

Table 1 shows physical and thermodynamic properties containing the dipole moment, thermal energy (ΔE°), thermal enthalpy (ΔH°), Gibbs free energy (ΔG°), and entropy (S°). The values of various thermodynamic properties and dipole moments of benzotriazole,

2-mercaptobenzothiazole, 8-hydroxyquinoline, and 3-amino-1,2,4-triazole-5-thiol adsorbed on the Al-Mg-Si were enhanced by increasing the molecular weight of these compounds and the charge distribution between organic compounds (electron donor) and the surface (electron acceptor) (Table 1) [51].

As shown in Figure 2, ΔG^{o}_{ads} may depend on the interactions between the inhibiting agents and the Al alloy surfaces. In fact, a comparison to ΔG^{o}_{ads} was in good accordance with the calculated results and the validity of the picked isotherm for the adsorption procdure of benzotriazole → Al-Mg-Si, 2-mercaptobenzothiazole → Al-Mg-Si, 8-hydroxyquinoline → Al-Mg-Si, and 3-amino-1,2,4-triazole-5-thiol → Al-Mg-Si (Figure 2).

$$\Delta G^{o}_{ads} \text{ amounts : } \Delta G^{o}_{ads} = \Delta G^{o}_{inh \to [Al-Mg-Si]} - \left(\Delta G^{o}_{inh} + \Delta G^{o}_{[Al-Mg-Si]}\right).$$

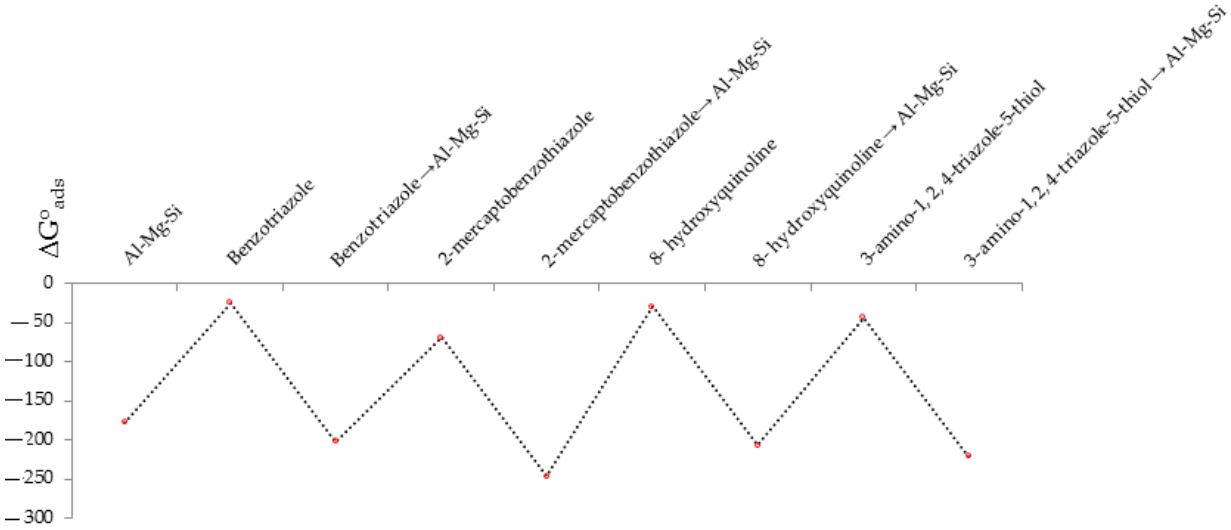

Figure 2. Gibbs free energy of benzotriazole, 2-mercaptobenzothiazole, 8-hydroxyquinoline, and 3-amino-1,2,4-triazole-5-thiol as corrosion inhibitors on the Al-Mg-Si alloy surface in NaCl solution at 300 K.

On the basis of data in Table 1, we predicted that the adsorption of the inhibitor on the Al-Mg-Si alloy surface might be physical and chemical in nature. As shown in Figure 2, all the computed ΔG^{o}_{ads} amounts were very close, which exhibited the agreement of the evaluated data by all methods and the validity of the computations; this also represented the maximum fluctuation for benzotriazole → Al-Mg-Si, 2-mercaptobenzothiazole → Al-Mg-Si, 8-hydroxyquinoline → Al-Mg-Si, and 3-amino-1,2,4-triazole-5-thiol → Al-Mg-Si (Figure 2).

3.2. "NMR" Spectroscopy & "NBO" Analysis

The heterocyclic organic inhibitors of benzotriazole, 2-mercaptobenzothiazole, 8-hydroxyquinoline, and 3-amino-1,2,4-triazole-5-thiol showed an approximately identical behavior (20–200 ppm) for various atoms in the active sites of these compounds through the "NMR" properties and electrostatic potential "ESP" surface (Figure 3a–d,a'–d'). The strongest peak was seen at almost 20 ppm for these components. The weakest peaks appeared at 120–140 ppm for all four heterocyclic carbenes, which consisted of benzotriazole, 2-mercaptobenzothiazole, 8-hydroxyquinoline, and 3-amino-1,2,4-triazole-5-thiol (Figure 3a–d).

Langmuir adsorbing of benzotriazole → Al-Mg-Si, 2-mercaptobenzothiazole → Al-Mg-Si, 8-hydroxyquinoline → Al-Mg-Si, and 3-amino-1,2,4-triazole-5-thiol → Al-Mg-Si showed band wavelengths between 10 ppm and 1000 ppm, and the sharpest peaks were at about 10 ppm for these compounds (Figure 3a'–d').

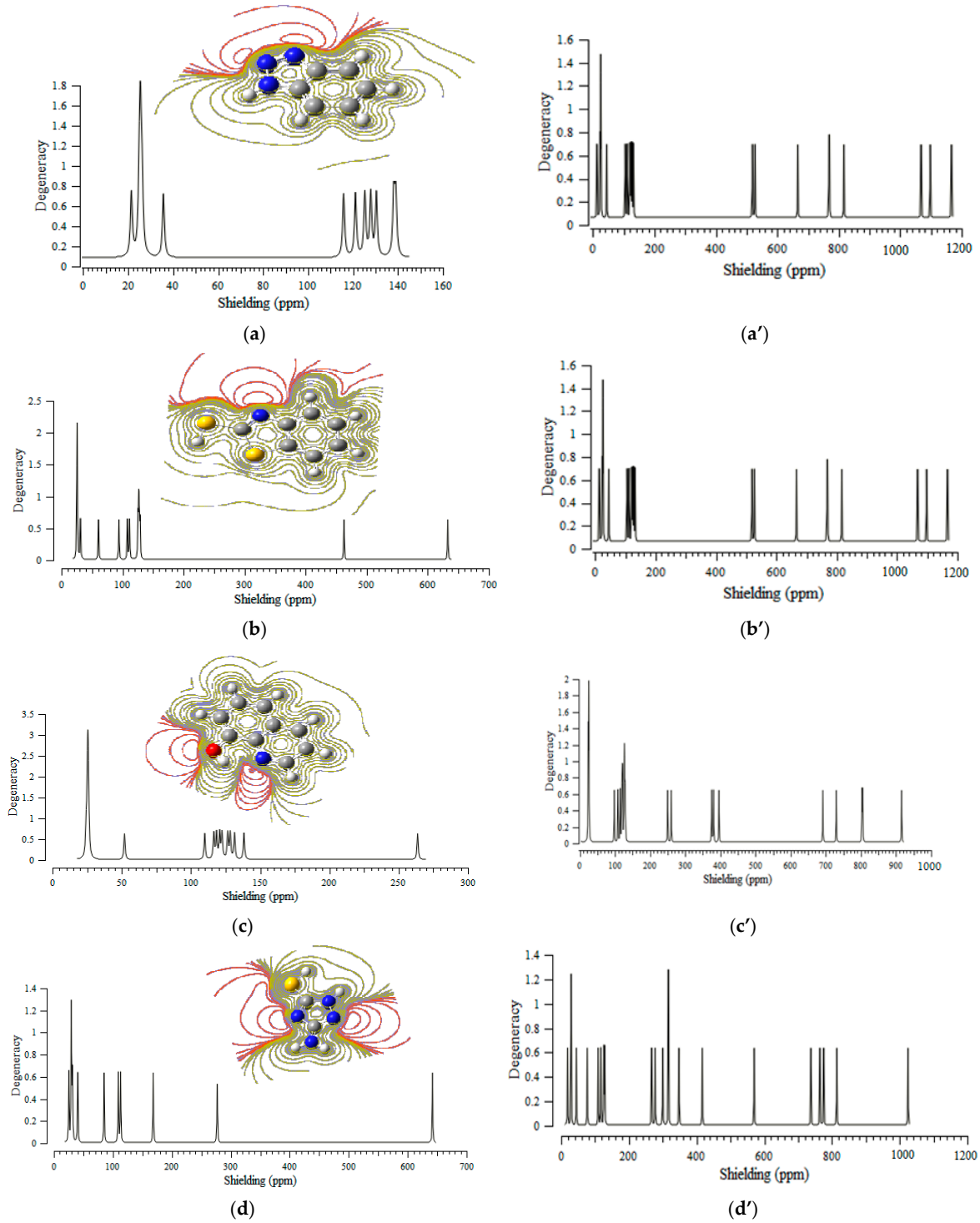

Figure 3. Chemical shift of "NMR" spectroscopy for (**a**) benzotriazole, (**a′**) benzotriazole → Al-Mg-Si, (**b**) 2-mercaptobenzothiazole, (**b′**) 2-mercaptobenzothiazole → Al-Mg-Si, (**c**) 8-hydroxyquinoline, (**c′**) 8-hydroxyquinoline → Al-Mg-Si, (**d**) 3-amino-1,2,4-triazole-5-thiol, and (**d′**) 3-amino-1,2,4-triazole-5-thiol → Al-Mg-Si indicating the active nitrogen, oxygen, and sulfur atoms in heterocyclic compounds approaching the nanosurface.

Then, the atomic charge and "NMR" data of the isotropic (σ_{iso}) and anisotropic shielding tensor (σ_{aniso}) for benzotriazole → Al-Mg-Si, 2-mercaptobenzothiazole → Al-Mg-Si, 8-hydroxyquinoline → Al-Mg-Si, and 3-amino-1,2,4-triazole-5-thiol → Al-Mg-Si were

calculated using Gaussian 16 revision C.01 software [35]; the results are reported in Table 2 [52–54].

Table 2. Atomic charge (Q) and NMR properties of some atoms of benzotriazole, 2-mercaptobenzothiazole, 8-hydroxyquinoline, and 3-amino-1,2,4-triazole-5-thiol in ppm adsorbed onto the Al-Mg-Si alloy surface.

Benzotriazole → Al-Mg-Si				**2-Mercaptobenzothiazole → Al-Mg-Si**			
Atom Number	**σ_{CSI}**	**σ_{CSA}**	**Q**	**Atom Number**	**σ_{CSI}**	**σ_{CSA}**	**Q**
C1	120.1330	144.3464	−0.0637	C1	139.2936	118.4161	−0.0018
C2	111.6339	155.5331	−0.0175	C2	134.3232	132.1443	−0.0112
C3	131.8879	138.7716	0.0136	C3	148.8807	101.7628	−0.2356
C4	105.1883	60.8572	0.0406	C4	133.1030	92.2893	0.0725
C5	127.8178	132.3853	0.0024	C5	134.1798	130.9800	0.0100
C6	123.9381	127.4240	−0.0234	C6	132.5749	132.8525	−0.0102
N7	−39.3745	222.1133	−0.247	S7	615.2211	352.1280	0.4900
N8	13.1291	127.7184	−0.0999	C8	66.1362	138.3513	−0.2058
N9	44.6789	320.9807	−0.1693	N9	39.3993	400.5662	−0.284
Al10	527.3315	712.2620	0.0942	S10	354.0150	388.3150	0.1054
Mg11	769.6581	592.7806	0.4635	Al11	228.9590	2775.1147	0.0704
Si12	−608.0968	2457.1321	−0.4390	Mg12	834.6620	650.3278	0.4803
Mg13	666.7797	717.9599	0.7295	Si13	−457.2518	1719.0572	−0.4733
Al14	768.3930	461.6928	0.1156	Mg14	626.0499	1179.7632	0.6134
Mg15	816.8921	478.5109	0.4296	Al15	488.4102	1924.5029	0.1084
Al16	1067.9909	975.1162	−0.3120	Mg16	756.9811	356.8803	0.4321
Si17	−488.2296	3646.7563	−1.1411	Al17	1074.2272	1028.1791	−0.5734
Al18	1098.0553	2400.1735	0.2054	Si18	−335.5606	2228.3322	−1.1356
Si19	−518.5837	2423.5913	−0.4705	Al19	1000.8690	1408.4209	0.1846
Mg20	519.2923	858.5605	0.6638	Si20	−302.5180	1660.6930	−0.4673
Al21	1167.0007	1138.1298	0.2251	Mg21	391.2234	404.0777	0.6367
				Al22	838.8937	1929.8643	0.1949
8-Hydroxyquinoline → Al-Mg-Si				3-Amino-1,2,4-triazole-5-thiol → Al-Mg-Si			
Atom Number	σ_{CSI}	σ_{CSA}	Q	Atom Number	σ_{CSI}	σ_{CSA}	Q
C1	98.2089	109.2773	0.0939	N1	77.0484	227.5978	−0.3065
C2	126.2638	128.7805	−0.0305	C2	109.2738	97.4358	0.2157
C3	119.4349	124.5888	0.0367	C3	117.4891	102.6288	0.0089
C4	126.8781	157.6865	−0.0100	N4	128.5710	161.4324	−0.0206
C5	129.3314	119.3934	−0.0304	N5	44.8980	178.5759	−0.2241
C6	121.8894	140.4467	−0.0034	N6	277.7289	33.8810	0.0444
N7	−1.6112	512.5816	−0.2439	S7	416.9395	177.8080	0.2172
C8	115.2833	117.7650	0.0802	Al8	347.9027	1045.3311	0.0620
C9	127.4460	138.5220	−0.0137	Mg9	764.3023	425.9930	0.4335
C10	121.2916	130.8941	0.0016	Si10	300.1406	902.6077	−0.4546
O11	108.4330	157.2175	−0.2988	Mg11	267.3292	311.3249	0.6178
Al12	249.7855	1244.5228	0.0838	Al12	316.7179	1168.7261	0.0707
Mg13	805.0097	564.9219	0.4314	Mg13	775.5928	350.3979	0.3697
Si14	−76.8544	1207.2367	−0.4547	Al14	1024.7125	697.9996	−0.4594
Mg15	380.5230	507.1433	0.6633	Si15	570.2486	760.7295	−1.2003
Al16	260.0607	1196.8740	0.0732	Al16	814.3200	922.1621	0.2166
Mg17	802.8973	597.2516	0.457	Si17	125.9742	1050.2575	−0.4388
Al18	915.6991	955.5742	−0.1330	Mg18	316.7269	394.5525	0.6466
Si19	375.3585	1390.2566	−1.2295	Al19	737.7535	1175.3999	0.2012
Al20	691.5878	1429.5138	0.2056				
Si21	−8.4049	1172.9932	−0.5003				
Mg22	395.8393	532.3253	0.6220				
Al23	729.9004	1438.6777	0.1992				

In addition, the NaCl solution influenced the electromagnetic traits of carbon, nitrogen, oxygen, sulfur, aluminum, magnesium, and silicon in benzotriazole → Al-Mg-Si, 2-mercaptobenzothiazole → Al-Mg-Si, 8-hydroxyquinoline → Al-Mg-Si, and 3-amino-1,2,4-triazole-5-thiol → Al-Mg-Si. Figure 4 indicates the isotropic (σ_{CSI}) and anisotropic (σ_{CSA}) chemical shielding tensors of some effective atoms on the adsorption sites of benzotriazole → Al-Mg-Si, 2-mercaptobenzothiazole → Al-Mg-Si, 8-hydroxyquinoline → Al-Mg-Si, and 3-amino-1,2,4-triazole-5-thiol → Al-Mg-Si (Table 2 and Figure 4).

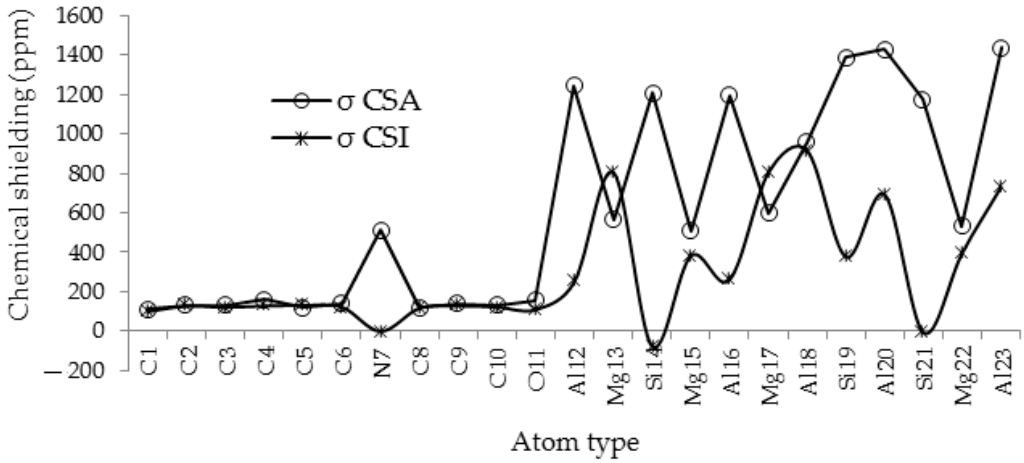

Figure 4. Isotropic (σ_{iso}) and anisotropic (σ_{aniso}) shielding tensors through intra-atomic interactions with magnesium and silicon atoms on the alloy surface of Al-Mg-Si and interatomic interaction with organic inhibitors on the adsorption site of «N → Al, O → Al, S → Al».

Interatomic interactions, which are related positions of one, two, three, etc. atoms at a time, are written as a series expansion of functional parameters with interatomic potential [54].

Intra-atomic interactions consisted of Al-Al, Al-Mg, Al-Si, Mg-Mg, Mg-Si, and Si-Si; interatomic interactions were N → Al-Mg-Si, O → Al-Mg-Si, and S → Al-Mg-Si based on the of CAM-B3LYP/6-31+G(d,p)/EPR-III/LANL2DZ quantum mechanics calculations using the Gaussian 16 revision C.01 program (Figure 4).

In Figure 4, it can be observed that Al-Si(14), Al-Si(19), and Al-Si(21) directed us to the most influence in the neighbor atoms generated by interatomic reactions of N →Al, O → Al, and S → Al on the Al-Mg-Si alloy surface. Furthermore, the natural bond orbital (NBO) analysis of benzotriazole, 2-mercaptobenzothiazole, 8-hydroxyquinoline, and 3-amino-1,2,4-triazole-5-thiol adsorbed on the Al-Mg-Si surface is reported in Table 3.

Table 3. NBO analysis of some atoms on the adsorption site for benzotriazole, 2-mercaptobenzothiazole, 8-hydroxyquinoline, and 3-amino-1,2,4-triazole-5-thiol bonded to the Al-Mg-Si alloy surface.

Heterocycles → Metal Alloy Surface	Bond Orbital	Occupancy	Hybrids
Benzotriazole → Al-Mg-Si	BD (1) N7—Al16	1.59462	0.9033 (π) N + 0.4289 ($sp^{2.20}$) Al
2-Mercaptobenzothiazole → Al-Mg-Si	BD (1) S10—Al17	1.75737	0.7996 (π) S + 0.6006 ($sp^{2.24}$) Al
8-Hydroxyquinoline → Al-Mg-Si	BD (1) O11—Al18	1.62010	0.6467 (π) O + 0.7628 ($sp^{2.07}$) Al
3-Amino-1,2,4-triazole-5-thiol → Al-Mg-Si	BD (1) S7—Al14	1.77439	0.7708 (π) S + 0.6371 ($sp^{2.56}$) Al

In Table 3, the benzotriazole, 2-mercaptobenzothiazole, 8-hydroxyquinoline, and 3-amino-1,2,4-triazole-5-thiol adsorbed on the Al-Mg-Si indicate the electron donor atoms bonded to the aluminum atom as the electron acceptor on the alloy surface at the active site area. The bond orbitals of S7—Al14 in 3-amino-1,2,4-triazole-5-thiol → Al-Mg-Si, S10—Al17

in 2-mercaptobenzothiazole → Al-Mg-Si, O11—Al18 in 8-hydroxyquinoline → Al-Mg-Si, and N7—Al16 in Benzotriazole → Al-Mg-Si showed the maximum occupancy.

3.3. Nuclear Quadrupole Resonance ("NQR")

The nuclear quadrupole resonance (NQR) frequency for benzotriazole → Al-Mg-Si, 2-mercaptobenzothiazole → Al-Mg-Si, 8-hydroxyquinoline → Al-Mg-Si, and 3-amino-1,2,4-triazole-5-thiol → Al-Mg-Si was measured (Table 4). There was an electric quadrupole moment that was accompanied by non-spherical nuclear charge distributions. So, the nuclear charge distribution deviated from that of a sphere as the oblate or prolate form of the nucleus [55–58]. In this research work, the electric potential was measured for benzotriazole, 2-mercaptobenzothiazole, 8-hydroxyquinoline, and 3-amino-1,2,4-triazole-5-thiol diffusing onto an Al-Mg-Si alloy surface (Table 4).

Table 4. Electric potential for elements of benzotriazole, 2-mercaptobenzothiazole, 8-hydroxyquinoline, and 3-amino-1,2,4-triazole-5-thiol adsorbed on the Al-Mg-Si alloy surface according to a "CAM-B3LYP/EPR-III,6-31+G(d,p)" calculation extracted from the "NQR" method.

Atom Type	Benzotriazole	Atom Type	2-Mercapto-benzothiazole	Atom Type	8-Hydroxy-quinoline	Atom Type	3-Amino-1,2,4-triazole-5-thiol
C1	−14.6152	C1	−14.5599	C1	−14.506	N1	−18.1871
C2	−14.5807	C2	−14.5697	C2	−14.5761	C2	−14.4916
C3	−14.5397	C3	−14.5643	C3	−14.5404	C3	−14.5524
C4	−14.5511	C4	−14.5341	C4	−14.557	N4	−18.0542
C5	−14.571	C5	−14.5706	C5	−14.5865	N5	−18.1750
C6	−14.5828	C6	−14.5707	C6	−14.5682	N6	−18.0540
N7	−18.1148	S7	−58.2774	N7	−18.1317	S7	−58.3546
N8	−18.0989	C8	−14.5665	C8	−14.5394	Al8	−43.7470
N9	−18.1089	N9	−18.1352	C9	−14.5679	Mg9	−38.70415
Al10	−43.7244	S10	−58.445	C10	−14.5631	Si10	−48.3056
Mg11	−38.7017	Al11	−43.7471	O11	−22.0527	Mg11	−38.9665
Si12	−48.2798	Mg12	−38.6987	Al12	−43.7399	Al12	−43.7520
Mg13	−38.9456	Si13	−48.3095	Mg13	−38.716	Mg13	−38.6765
Al14	−43.7191	Mg14	−38.9819	Si14	−48.3057	Al14	−43.2490
Mg15	−38.7164	Al15	−43.7426	Mg15	−38.9685	Si15	−48.0739
Al16	−43.26	Mg16	−38.7278	Al16	−43.7423	Al16	−43.5918
Si17	−48.0142	Al17	−43.2854	Mg17	−38.7179	Si17	−48.3095
Al18	−43.595	Si18	−48.0619	Al18	−43.2654	Mg18	−38.975
Si19	−48.2863	Al19	−43.6228	Si19	−48.0458	Al19	−43.6124
Mg20	−38.9298	Si20	−48.3171	Al20	−43.602		
Al21	−43.6121	Mg21	−38.9744	Si21	−48.3141		
		Al22	−43.623	Mg22	−38.9765		
				Al23	−43.6074		

In addition, Figure 5a–d show the electric potential for elements of benzotriazole, 2-mercaptobenzothiazole, 8-hydroxyquinoline, and 3-amino-1,2,4-triazole-5-thiol that were adsorbed onto the Al-Mg-Si alloy.

Figure 5 shows the electric potential for carbon, nitrogen, oxygen, sulfur, aluminum, magnesium, and silicon in benzotriazole → Al-Mg-Si, 2-mercaptobenzothiazole → Al-Mg-Si, 8-hydroxyquinoline → Al-Mg-Si, and 3-amino-1,2,4-triazole-5-thiol → Al-Mg-Si.

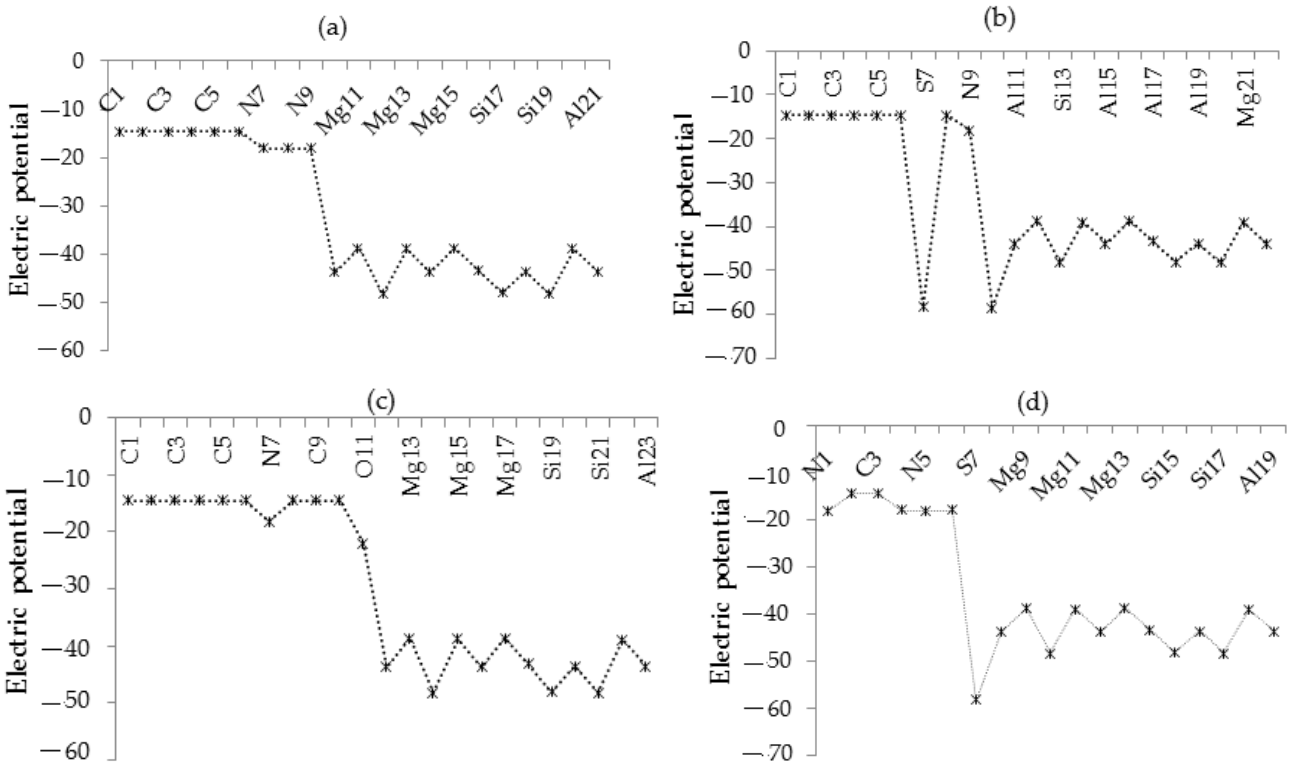

Figure 5. Electric potential for (**a**) benzotriazole, (**b**) 2-mercaptobenzothiazole, (**c**) 8-hydroxyquinoline, and (**d**) 3-amino-1,2,4-triazole-5-thiol adsorbed onto the Al-Mg-Si alloy.

3.4. Charge Density Analysis

By observing the intra/interatomic interactions between the organic inhibitor of benzotriazole, 2-mercaptobenzothiazole, 8-hydroxyquinoline, and 3-amino-1,2,4-triazole-5-thiol with the Al-Mg-Si alloy surface and the consequent formation of adsorbed surfaces of benzotriazole → Al-Mg-Si, 2-mercaptobenzothiazole→ Al-Mg-Si, 8-hydroxyquinoline → Al-Mg-Si, and 3-amino-1,2,4-triazole-5-thiol → Al-Mg-Si (Table 2), the charge density difference ("CDD") for these structures at the adsorption site was estimated and plotted as shown in Figure 6.

Figure 6. Calculated electronic charge for aluminum atoms through intra-atomic interactions with magnesium and silicon on the alloy surface of Al-Mg-Si and through interatomic interactions with organic inhibitors on the adsorption site of «N → Al, O → Al, S → Al».

Furthermore, the presence of covalent bonds in this alloy exhibited the identical energy value and outlook of the "PDOS" for the *p* orbitals of aluminum and silicon (Figure 7).

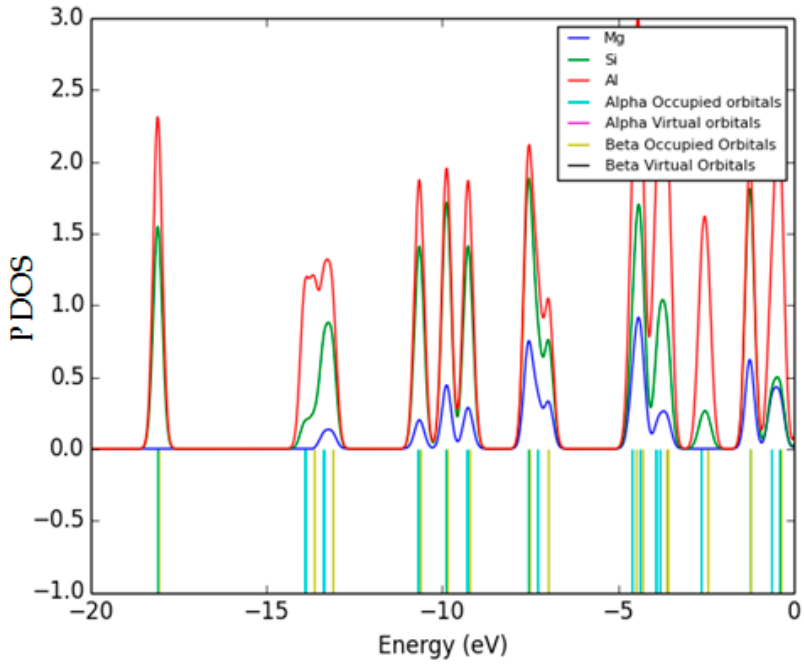

Figure 7. PDOS of Al-Mg-Si alloy surface with Fermi level = 0.

Furthermore, the Al-Mg-Si alloy surface showed an atomic charge (coulomb) of −1.200 before adsorption of heterocyclic carbenes and −1.41, −1.136, −1.230, and −0.407 after adsorption of benzotriazole, 2-mercaptobenzothiazole, 8-hydroxyquinoline, and 3-amino-1,2,4-triazole-5-thiol, respectively. Therefore, the charge densities for benzotriazole, 2-mercaptobenzothiazole, 8-hydroxyquinoline, and 3-amino-1,2,4-triazole-5-thiol on the Al-Mg-Si alloy surface were alternatively: $\Delta Q_{\text{3-amino-1,2,4-triazole-5-thiol} \rightarrow \text{Al-Mg-Si}} = 0.793 > \Delta Q_{\text{2-mercaptobenzothiazole} \rightarrow \text{Al-Mg-Si}} = 0.064 > \Delta Q_{\text{8-hydroxyquinoline} \rightarrow \text{Al-Mg-Si}} = -0.03 > \Delta Q_{\text{benzotriazole} \rightarrow \text{Al-Mg-Si}} = -0.21$. The data explain the charge penetration through adsorption of benzotriazole on the Al-Mg-Si alloy surface.

3.5. Potential Energy of Interatomic Interactions

When binding occurred, we could observe the potential with both an attractive and a repulsive component [59]. Therefore, the optimized potential energies of the interatomic interaction for benzotriazole → Al-Mg-Si, 2-mercaptobenzothiazole → Al-Mg-Si, 8-hydroxyquinoline → Al-Mg-Si, and 3-amino-1,2,4-triazole-5-thiol → Al-Mg-Si were measured (Table 5).

Table 5. Potential energy (kcal/mol) for benzotriazole, oxygen atom in 8-hydroxyquinoline, and sulfur atom in both 2-mercaptobenzothiazole and 3-amino-1,2,4-triazole-5-thiol with aluminum on the Al-Mg-Si nanosurface.

Compound	**Potential Energy × 10^{-4} (kcal/mol)**	**Distance**	**(Å)**
Al-Mg-Si	−177.5928	-	-
Benzotriazole	−24.5172	-	-
Benzotriazole → Al-Mg-Si	−202.0580	$N_{\text{adsorbate}} \rightarrow Al_{\text{surface}}$	1.9518
2-Mercaptobenzothiazole	−69.5235	-	-
2-Mercaptobenzothiazole → Al-Mg-Si	−247.0476	$S_{\text{adsorbate}} \rightarrow Al_{\text{surface}}$	2.1998
8-Hydroxyquinoline	−29.5527	-	-
8-Hydroxyquinoline → Al-Mg-Si	−207.1047	$O_{\text{adsorbate}} \rightarrow Al_{\text{surface}}$	1.9098
3-Amino-1,2,4-triazole-5-thiol	−43.1337	-	-
3-Amino-1,2,4-triazole-5-thiol → Al-Mg-Si	−220.6679	$S_{\text{adsorbate}} \rightarrow Al_{\text{surface}}$	2.1998

Then, the distance between the nitrogen atom in benzotriazole, oxygen atom in 8-hydroxyquinoline, and sulfur atom in both 2-mercaptobenzothiazole and 3-amino-1,2,4-triazole-5-thiol with aluminum on the Al-Mg-Si nanosurface was evaluated (Table 5 and Figure 8).

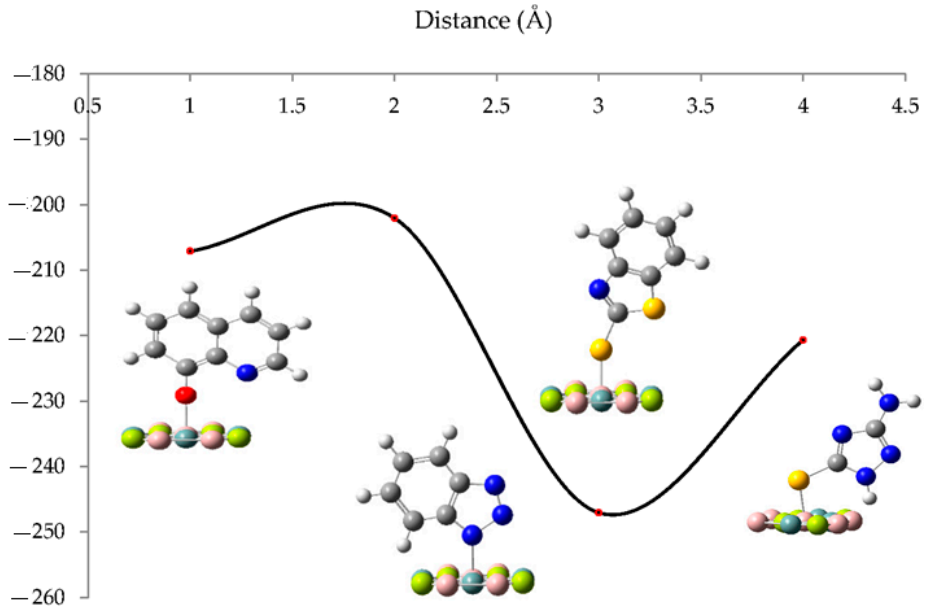

Figure 8. Potential energy (kcal/mol) for benzotriazole, oxygen atom in 8-hydroxyquinoline, and sulfur atom in both 2-mercaptobenzothiazole and 3-amino-1,2,4-triazole-5-thiol with aluminum on the Al-Mg-Si nanosurface.

Based on Figure 8, we assumed that for benzotriazole → Al-Mg-Si, 2-mercapto-benzothiazole → Al-Mg-Si, 8-hydroxyquinoline → Al-Mg-Si, and 3-amino-1,2,4-triazole-5-thiol → Al-Mg-Si, the Lennard-Jones potential as an intermolecular pair potential can be described [60,61].

3.6. "HOMO", "LUMO", and "UV-vis" Analysis

Ionization causes the highest occupied molecular orbital ("HOMO") energy, and the electron affinity produces the lowest unoccupied molecular orbital ("LUMO") energy, which were calculated and reported for benzotriazole → Al-Mg-Si, 2-mercaptobenzothiazole → Al-Mg-Si, 8-hydroxyquinoline → Al-Mg-Si, and 3-amino-1,2,4-triazole-5-thiol → Al-Mg-Si (Scheme 3). The "HOMO" (au), "LUMO" (au), and band energy gap "$\Delta E = E_{LUMO} - E_{HOMO}$" (ev) present a pictorial explanation of the frontier molecular orbitals and their respective positive and negative zones, which were important factors in identifying the molecular characteristics of effective compounds in these organic inhibitors (Scheme 3).

In fact, the compositions with a half-filled "HOMO-LUMO" band were not only metallic but could also turn to semiconducting, in which a molecular material is known to enter the zero-resistance state encountered for Al-Mg-Si toward adsorption of organic heterocyclic carbenes. The chemical reactivity of Al-Mg-Si was conducted by its low "HOMO–LUMO" gap, making it an appropriate electron acceptor. The energy gap between "HOMO" and "LUMO" distinguished the attributes of molecular electrical transport [62]. Based on the "Franck–Condon" principle, the maximum absorption peak (max) depends on a UV–visible spectrum of vertical excitation [63–67].

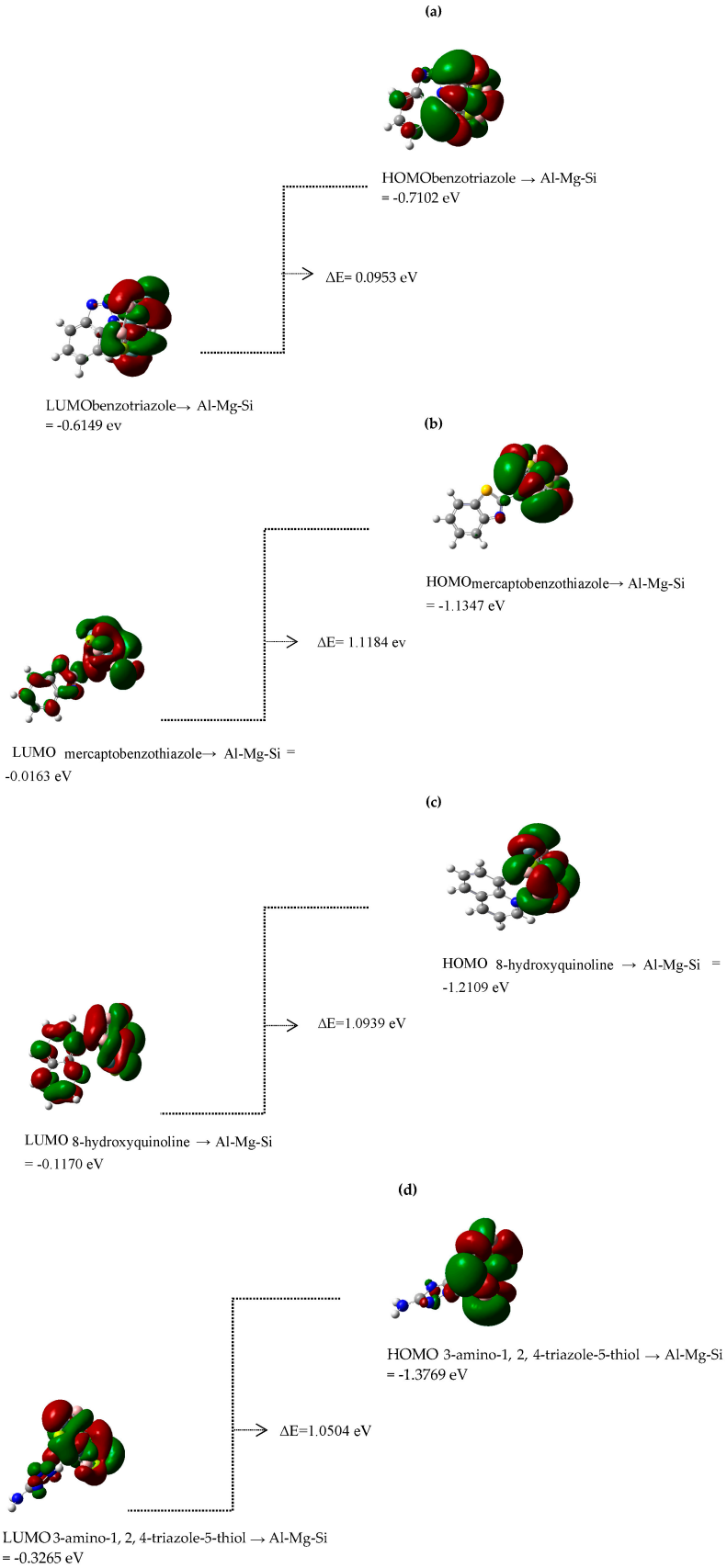

Scheme 3. The HOMO, LUMO, and band energy gap (ev) for three organic inhibitors for (**a**) benzotriazole → Al-Mg-Si, (**b**) 2-mercaptobenzothiazole, (**c**) 8-hydroxyquinoline, and (**d**) 3-amino-1,2,4-triazole-5-thiol → Al-Mg-Si.

Finally, "TD-DFT/6-31+G (2d,p)/EPR-III/LANL2DZ" computation which has been a computational QM modelling methodology for studying the electronic structure of many-body systems [49,68–72], was done to identify the low-lying excited states of benzotriazole, 8-hydroxyquinoline, 2-mercaptobenzothiazole, and 3-amino-1,2,4-triazole-5-thiol adsorbing on the Al-Mg-Si alloy surface. The data contained the vertical excitation energies, oscillator strengths, and wavelengths, which are shown in Figure 9a–d.

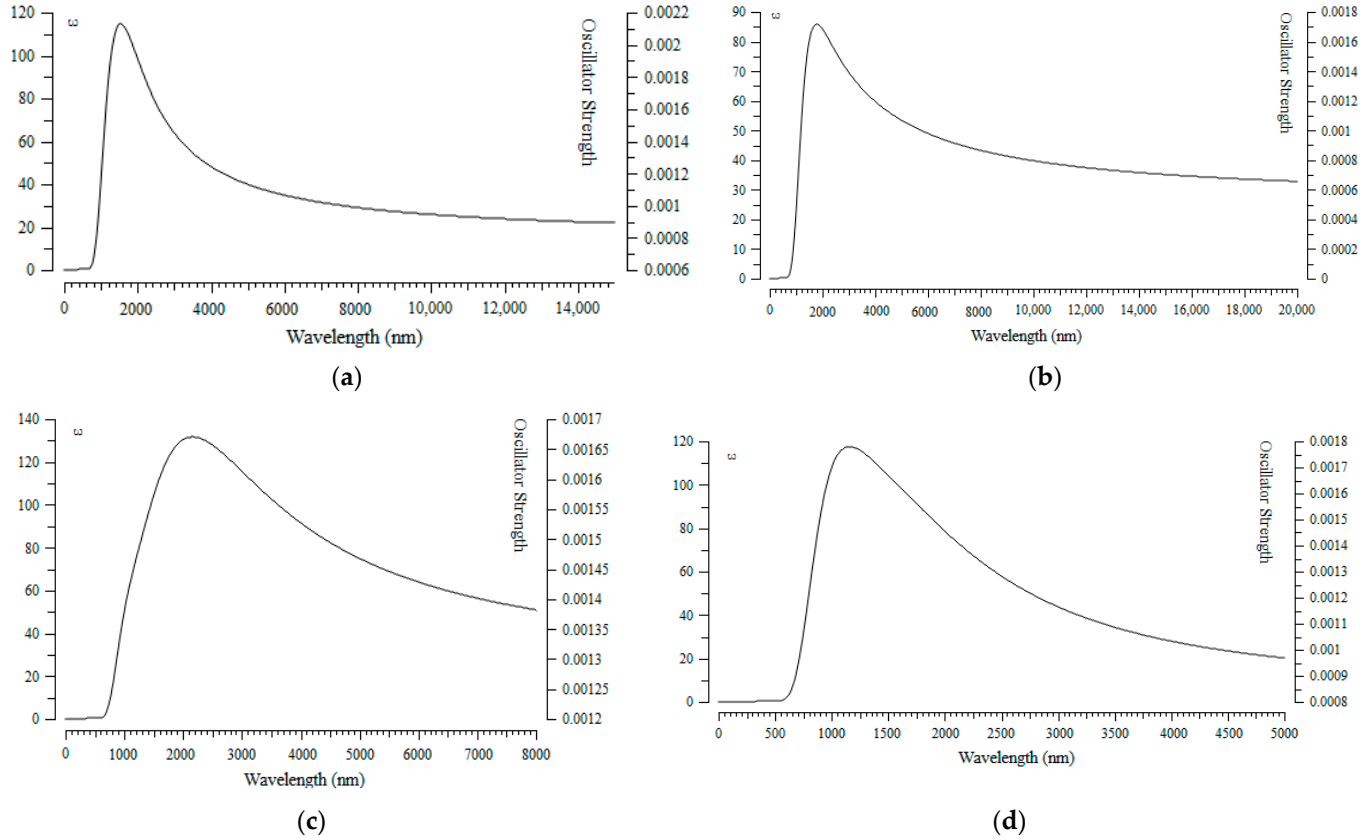

Figure 9. "UV-vis" spectra for (**a**) benzotriazole → Al-Mg-Si, (**b**) 2-mercaptobenzothiazole, (**c**) 8-hydroxyquinoline, and (**d**) 3-amino-1,2,4-triazole-5-thiol → Al-Mg-Si.

As a matter of fact, based on the calculated values of the "UV-vis" spectra for benzotriazole, 2-mercaptobenzothiazole, 8-hydroxyquinoline, and 3-amino-1,2,4-triazole-5-thiol adsorbing onto the Al-Mg-Si alloy surface, there were maximum adsorption bands in the range of 1000–3000 nm wavelengths for these organic heterocyclic inhibitors of the joint metal alloy; these showed a sharp peak with an approximately 2000 nm wavelength (Figure 9a–d).

4. Conclusions

In this work, the adsorption and diffusion of benzotriazole, 2-mercaptobenzothiazole, 8-hydroxyquinoline, and 3-amino-1,2,4-triazole-5-thiol adsorbed onto an Al-Mg-Si alloy surface were studied based on the "Langmuir" theory using the "ONIOM" method with "high", "medium", and "low" levels of "EPR-III/6-31+G (d,p)/LANL2DZ" as well as semi-empirical and "MM2" basis sets using the program package "Gaussian 16" revision C.01.

In this research, the effectiveness of the (N- and S-) heterocycles as the Al alloy coating was investigated through the electromagnetic traits, a thermodynamic analysis, and characteristics of the environmental situation, which resulted in the complexes of benzotriazole → Al-Mg-Si, 2-mercaptobenzothiazole → Al-Mg-Si, 8-hydroxyquinoline → Al-Mg-Si, and 3-amino-1,2,4-triazole-5-thiol → Al-Mg-Si.

A special investigation of the mechanism of local minima in the adsorption potential energy insight denoted that the intact benzotriazole, 2-mercaptobenzothiazole, 8-hydroxyquinoline, and 3-amino-1,2,4-triazole-5-thiol were adsorbed with the aromatic ring parallel to the Al-Mg-Si alloy surface. In the favorite path, these (N- and S-) heterocycles remained parallel to the surface while running small single rotational steps with a "C–C" double-bond hinged top of a single Al element.

Author Contributions: F.M.: Conceptualization and idea, Methodology, Software, Validation, Formal analysis, Investigation, Data curation, Writing—original draft preparation, visualization, Supervision, Project administration. M.M.: Methodology, Software, Formal analysis, Investigation, Data curation, Writing—review and editing, Visualization, Resources. All authors have read and agreed to the published version of the manuscript.

Funding: This research received no external funding.

Data Availability Statement: Not applicable.

Acknowledgments: In successfully completing this paper and its research, the authors are grateful to Kastamonu University for its support through the library, the laboratory, and scientific websites.

Conflicts of Interest: The authors declare no conflict of interest.

References

1. Lasagni, F.; Lasagni, A.; Marks, E.; Holzapfel, C.; Mücklich, F.; Degischer, H. Three-dimensional characterization of 'as-cast' and solution-treated $AlSi_{12}$(Sr) alloys by high-resolution FIB tomography. *Acta Mater.* **2007**, *55*, 3875–3882. [CrossRef]
2. Mollaamin, F.; Monajjemi, M. Molecular modelling framework of metal-organic clusters for conserving surfaces: Langmuir sorption through the TD-DFT/ONIOM approach. *Mol. Simul.* **2023**, *49*, 365–376. [CrossRef]
3. Requena, G.; Garcés, G.; Rodríguez, M.; Pirling, T.; Cloetens, P. 3D architecture and load partition in eutectic Al-Si alloys. *Adv. Eng. Mater.* **2009**, *11*, 1007–1014. [CrossRef]
4. Mollaamin, F.; Monajjemi, M. In Silico-DFT Investigation of Nanocluster Alloys of Al-(Mg, Ge, Sn) Coated by Nitrogen Heterocyclic Carbenes as Corrosion Inhibitors. *J. Clust. Sci.* **2023**, 1–18. [CrossRef]
5. Asghar, Z.; Requena, G.; Kubel, F. The role of Ni and Fe aluminides on the elevated temperature strength of an $AlSi_{12}$ alloy. *Mater. Sci. Eng. A* **2010**, *527*, 5691–5698. [CrossRef]
6. Mollaamin, F.; Shahriari, S.; Monajjemi, M.; Khalaj, Z. Nanocluster of Aluminum Lattice via Organic Inhibitors Coating: A Study of Freundlich Adsorption. *J. Clust. Sci.* **2023**, *34*, 1547–1562. [CrossRef]
7. Stadler, F.; Antrekowitsch, H.; Fragner, W.; Kaufmann, H.; Uggowitzer, P. Effect of main alloying elements on strength of Al–Si foundry alloys at elevated temperatures. *Int. J. Cast Met. Res.* **2012**, *25*, 215–224. [CrossRef]
8. Boughoues, Y.; Benamira, M.; Messaadia, L.; Ribouh, N. Adsorption and corrosion inhibition performance of some environmental friendly organic inhibitors for mild steel in HCl solution via experimental and theoretical study. *Colloids Surf. A Physicochem. Eng. Asp.* **2020**, *593*, 124610. [CrossRef]
9. Mollaamin, F.; Monajjemi, M. Harmonic Linear Combination and Normal Mode Analysis of Semiconductor Nanotubes Vibrations. *J. Comput. Theor. Nanosci.* **2015**, *12*, 1030–1039. [CrossRef]
10. Monajjemi, M.; Noei, M.; Mollaamin, F. Design of fMet-tRNA and Calculation of its Bonding Properties by Quantum Mechanics. *Nucleosides Nucleotides Nucleic Acids* **2010**, *29*, 676–683. [CrossRef]
11. Guimarães, T.A.; da Cunha, J.N.; de Oliveira, G.A.; da Silva, T.U.; de Oliveira, S.M.; de Araújo, J.R.; Machado, S.d.P.; D'Elia, E.; Rezende, M.J. Nitrogenated derivatives of furfural as green corrosion inhibitors for mild steel in HCl solution. *J. Mater. Res. Technol.* **2020**, *9*, 7104–7122. [CrossRef]
12. Monajjemi, M.; Mahdavian, L.; Mollaamin, F. Characterization of nanocrystalline silicon germanium film and nanotube in adsorption gas by Monte Carlo and Langevin dynamic simulation. *Bull. Chem. Soc. Ethiop.* **2008**, *22*, 277–286. [CrossRef]
13. Mobin, M.; Aslam, R. Experimental and theoretical study on corrosion inhibition performance of environmentally benign nonionic surfactants for mild steel in 3.5% NaCl solution. *Process Saf. Environ. Prot.* **2018**, *114*, 279–295. [CrossRef]
14. Singh, A.; Lin, Y.; Quraishi, M.A.; Olasunkanmi, L.O.; Fayemi, O.E.; Sasikumar, Y.; Ramaganthan, B.; Bahadur, I.; Obot, I.B.; Adekunle, A.S.; et al. Porphyrins as corrosion inhibitors for N80 steel in 3.5% NaCl solution: Electrochemical, quantum chemical, QSAR and Monte Carlo simulations studies. *Molecules* **2015**, *20*, 15122–15146. [CrossRef]
15. Ali, S.A.; Mazumder, M.A.J.; Nazal, M.K.; Al-Muallem, H.A. Assembly of succinic acid and isoxazolidine motifs in a single entity to mitigate CO_2 corrosion of mild steel in saline media. *Arab. J. Chem.* **2020**, *13*, 242–257. [CrossRef]
16. Amar, H.; Benzakour, J.; Derja, A.; Villemin, D.; Moreau, B. A corrosion inhibition study of iron by phosphonic acids in sodium chloride solution. *J. Electroanal. Chem.* **2003**, *558*, 131–139. [CrossRef]
17. Monajjemi, M.; Khaleghian, M.; Tadayonpour, N.; Mollaamin, F. The effect of different solvents and temperatures on stability of single-walled carbon nanotube: A QM/MD study. *Int. J. Nanosci.* **2010**, *9*, 517–529. [CrossRef]

18. Mollaamin, F.; Noei, M.; Monajjemi, M.; Rasoolzadeh, R. Nano theoretical studies of fMET-tRNA structuren in protein synthesis of prokaryotes and its comparison with the structure of fALA-tRNA. *Afr. J. Microbiol. Res.* **2011**, *5*, 2667–2674. [CrossRef]
19. Yang, D.; Zhang, M.; Zheng, J.; Castaneda, H. Corrosion inhibition of mild steel by an imidazolium ionic liquid compound: The effect of pH and surface pre-corrosion. *RSC Adv.* **2015**, *5*, 95160–95170. [CrossRef]
20. Mollaamin, F.; Monajjemi, M. Tailoring and functionalizing the graphitic-like GaN and GaP nanostructures as selective sen-sors for NO, NO_2, and NH_3 adsorbing: A DFT study. *J. Mol. Model.* **2023**, *29*, 170. [CrossRef]
21. Mollaamin, F.; Monajjemi, M. Transition metal (X = Mn, Fe, Co, Ni, Cu, Zn)-doped graphene as gas sensor for CO_2 and NO_2 detection: A molecular modeling framework by DFT perspective. *J. Mol. Model.* **2023**, *29*, 119. [CrossRef] [PubMed]
22. Mollaamin, F.; Monajjemi, M. Doping of Graphene Nanostructure with Iron, Nickel and Zinc as Selective Detector for the Toxic Gas Removal: A Density Functional Theory Study. *C* **2023**, *9*, 20. [CrossRef]
23. Amberchan, G.; Lopez, I.; Ehlke, B.; Barnett, J.; Bao, N.Y.; Allen, A.L.; Singaram, B.; Oliver, S.R. Aluminum Nanoparticles from a Ga–Al Composite for Water Splitting and Hydrogen Generation. *ACS Appl. Nano Mater.* **2022**, *5*, 2636–2643. [CrossRef]
24. Mollaamin, F.; Monajjemi, M. Tribocorrosion Framework of (Iron, Nickel, Zinc)-Doped Graphene Nanosheet: New Sights into Sulfur Dioxide and Hydrogen Sulfide Removal Using DFT/TD-DFT Methods. *J. Bio-Tribo-Corros.* **2023**, *9*, 47. [CrossRef]
25. Monajjemi, M.; Farahani, N.; Mollaamin, F. Thermodynamic study of solvent effects on nanostructures: Phosphatidylserine and phosphatidylinositol membranes. *Phys. Chem. Liq.* **2012**, *50*, 161–172. [CrossRef]
26. Mollaamin, F.; Ilkhani, A.; Sakhaei, N.; Bonsakhteh, B.; Faridchehr, A.; Tohidi, S.; Monajjemi, M. Thermodynamic and solvent effect on dynamic structures of nano bilayer-cell membrane: Hydrogen bonding study. *J. Comput. Theor. Nanosci.* **2015**, *12*, 3148–3154. [CrossRef]
27. Xhanari, K.; Finšgar, M. Organic corrosion inhibitors for aluminum and its alloys in acid solutions: A review. *RSC Adv.* **2016**, *6*, 62833–62857. [CrossRef]
28. Mollaamin, F.; Monajjemi, M. Graphene Embedded with Transition Metals for Capturing Carbon Dioxide: Gas Detection Study Using QM Methods. *Clean Technol.* **2023**, *5*, 20. [CrossRef]
29. Mashuga, M.E.; Olasunkanmi, L.O.; Ebenso, E.E. Experimental and theoretical investigation of the inhibitory effect of new pyridazine derivatives for the corrosion of mild steel in 1M HCl. *J. Mol. Struct.* **2017**, *1136*, 127–139. [CrossRef]
30. Shahriari, S.; Soofi, N.S.; Farzi, F.; Attarikhasraghi, N.; Khosravi, S.; BabaeiTuskiee, B.; Esmkhani, R.; Monajjemi, M. Interaction of Nano-Boron Nitride/Graphene Sheets with Anode Lithium Ion Battery. *J. Comput. Theor. Nanosci.* **2016**, *13*, 3070–3082. [CrossRef]
31. Monajjemi, M.; Baie, M.T.; Mollaamin, F. Interaction between threonine and cadmium cation in [Cd(Thr)] (n = 1–3) complexes: Density functional calculations. *Russ. Chem. Bull.* **2010**, *59*, 886–889. [CrossRef]
32. Svensson, M.; Humbel, S.; Froese, R.D.J.; Matsubara, T.; Sieber, S.; Morokuma, K. ONIOM: A Multilayered Integrated MO + MM Method for Geometry Optimizations and Single Point Energy Predictions. A Test for Diels−Alder Reactions and $Pt(P(t\text{-}Bu)_3)_2$ + H_2 Oxidative Addition. *J. Phys. Chem.* **1996**, *100*, 19357–19363. [CrossRef]
33. Brandt, F.; Jacob, C.R. Systematic QM Region Construction in QM/MM Calculations Based on Uncertainty Quantification. *J. Chem. Theory Comput.* **2022**, *18*, 2584–2596. [CrossRef]
34. Dennington, R.; Keith, T.A.; Millam, J.M. *GaussView, Version 6*; Semichem Inc.: Shawnee Mission, KS, USA, 2016.
35. Frisch, M.J.; Trucks, G.W.; Schlegel, H.B.; Scuseria, G.E.; Robb, M.A.; Cheeseman, J.R.; Scalmani, G.; Barone, V.; Petersson, G.A.; Nakatsuji, H.; et al. *Gaussian 16, Revision C.01*; Gaussian, Inc.: Wallingford, CT, USA, 2016.
36. Andersen, S.J.; Marioara, C.D.; Vissers, R.; Frøseth, A.; Zandbergen, H.W. The structural relation between precipitates in AlMgSi alloys, the Al-matrix and diamond silicon, with emphasis on the trigonal phase U1- MgAl2Si2. *Mater. Sci. Eng. A* **2007**, *444*, 157–169. [CrossRef]
37. Bilić, A.; Reimers, J.R.; Hush, N.S. Adsorption of Pyridine on the Gold(111) Surface: Implications for "Alligator Clips" for Molecular Wires. *J. Phys. Chem. B* **2002**, *106*, 6740–6747. [CrossRef]
38. Malone, W.; Kara, A. A coverage dependent study of the adsorption of pyridine on the (111) coinage metal surfaces. *Surf. Sci.* **2020**, *693*, 121525. [CrossRef]
39. Monajjemi, M.; Mollaamin, F.; Gholami, M.R.; Yoosbashizadeh, H.; Sadrnezhad, S.K.; Passdar, H. Quantum Chemical Parameters of Some Organic Corrosion Inhibitors, Pyridine, 2-Picoline 4-Picoline and 2, 4- Lutidine, Adsorption at Aluminum Surface in Hydrocholoric and Nitric Acids and Comparison Between Two Acidic Media. *Main Group Met. Chem.* **2003**, *26*, 349–362. [CrossRef]
40. Dumont, E.; De Bleye, C.; Haouchine, M.; Coïc, L.; Sacré, P.-Y.; Hubert, P.; Ziemons, E. Effect of the functionalisation agent on the surface-enhanced Raman scattering (SERS) spectrum: Case study of pyridine derivatives. *Spectrochim. Acta Part A Mol. Biomol. Spectrosc.* **2020**, *233*, 118180. [CrossRef]
41. Mollenhauer, D.; Gaston, N.; Voloshina, E.; Paulus, B. Interaction of Pyridine Derivatives with a Gold (111) Surface as a Model for Adsorption to Large Nanoparticles. *J. Phys. Chem. C* **2013**, *117*, 4470–4479. [CrossRef]
42. Isvoranu, C.; Wang, B.; Ataman, E.; Schulte, K.; Knudsen, J.; Andersen, J.N.; Bocquet, M.-L.; Joachim Schnadt, J. Pyridine Adsorption on Single-Layer Iron Phthalocyanine on Au(111). *J. Phys. Chem. C* **2011**, *115*, 20201–20208. [CrossRef]
43. Becke, A.D. Density-functional thermochemistry. III. The role of exact exchange. *J. Chem. Phys.* **1993**, *98*, 5648–5652. [CrossRef]
44. Lee, C.; Yang, W.; Parr, R.G. Development of the Colle–Salvetti correlation-energy formula into a functional of the electron density. *Phys. Rev. B* **1988**, *37*, 785–789. [CrossRef] [PubMed]

45. Kim, K.; Jordan, K.D. Comparison of Density Functional and MP2 Calculations on the Water Monomer and Dimer. *J. Phys. Chem.* **1994**, *98*, 10089–10094. [CrossRef]
46. Stephens, P.J.; Devlin, F.J.; Chabalowski, C.F.; Frisch, M.J. Ab Initio Calculation of Vibrational Absorption and Circular Dichroism Spectra Using Density Functional Force Fields. *J. Phys. Chem.* **1994**, *98*, 11623–11627. [CrossRef]
47. Cramer, C.J. *Essentials of Computational Chemistry: Theories and Models*, 2nd ed.; Wiley: New York, NY, USA, 2004; Available online: wiley.com (accessed on 24 June 2021).
48. Monajjemi, M.; Falahati, M.; Mollaamin, F. Computational investigation on alcohol nanosensors in combination with carbon nanotube: A Monte Carlo and ab initio simulation. *Ionics* **2013**, *19*, 155–164. [CrossRef]
49. Shahriari, S.; Mollaamin, F.; Monajjemi, M. Increasing the Performance of {[(1 − x − y)$LiCo_{0.3}Cu_{0.7}$] (Al and Mg doped)]O_2}, $_xLi_2MnO_3$, y$LiCoO_2$ Composites as Cathode Material in Lithium-Ion Battery: Synthesis and Characterization. *Micromachines* **2023**, *14*, 241. [CrossRef]
50. Ghalandari, B.; Monajjemi, M.; Mollaamin, F. Theoretical Investigation of Carbon Nanotube Binding to DNA in View of Drug Delivery. *J. Comput. Theor. Nanosci.* **2011**, *8*, 1212–1219. [CrossRef]
51. Mollaamin, F.; Monajjemi, M.; Salemi, S.; Baei, M.T. A Dielectric Effect on Normal Mode Analysis and Symmetry of BNNT Nanotube. *Fuller. Nanotub. Carbon Nanostruct.* **2011**, *19*, 182–196. [CrossRef]
52. Bakhshi, K.; Mollaamin, F.; Monajjemi, M. Exchange and correlation effect of hydrogen chemisorption on nano V(100) surface: A DFT study by generalized gradient approximation (GGA). *J. Comput. Theor. Nanosci.* **2011**, *8*, 763–768. [CrossRef]
53. Tahan, A.; Mollaamin, F.; Monajjemi, M. Thermochemistry and NBO analysis of peptide bond: Investigation of basis sets and binding energy. *Russ. J. Phys. Chem. A* **2009**, *83*, 587–597. [CrossRef]
54. Monajjemi, M.; Khaleghian, M.; Mollaamin, F. Theoretical study of the intermolecular potential energy and second virial coefficient in the mixtures of CH4 and Kr gases: A comparison with experimental data. *Mol. Simul.* **2010**, *36*, 865–870. [CrossRef]
55. Smith, J.A.S. Nuclear Quadrupole Resonance Spectroscopy. *J. Chem. Educ.* **1971**, *48*, 39–41. [CrossRef]
56. Mollaamin, F.; Shahriari, S.; Monajjemi, M. Induced Metals on BN–Nanotube by DFT/EPR Methods. *Russ. J. Phys. Chem. A* **2021**, *95* (Suppl. S2), S331–S337. [CrossRef]
57. Mollaamin, F.; Monajjemi, M. Corrosion Inhibiting by Some Organic Heterocyclic Inhibitors Through Langmuir Adsorption Mechanism on the Al-*X* (*X* = Mg/Ga/Si) Alloy Surface: A Study of Quantum Three-Layer Method of CAM-DFT/ONIOM. *J. Bio Tribo Corros.* **2023**, *9*, 33. [CrossRef]
58. Young, H.A.; Freedman, R.D. *Sears and Zemansky's University Physics with Modern Physics*, 13th ed.; Addison-Wesley: Boston, MA, USA, 2012; p. 754.
59. Monajjemi, M.; Khosravi, M.; Honarparvar, B.; Mollaamin, F. Substituent and solvent effects on the structural bioactivity and anticancer characteristic of catechin as a bioactive constituent of green tea. *Int. J. Quantum Chem.* **2011**, *111*, 2771–2777. [CrossRef]
60. Heinz, H.; Vaia, R.A.; Farmer, B.L.; Naik, R.R. Accurate Simulation of Surfaces and Interfaces of Face-Centered Cubic Metals Using 12-6 and 9-6 Lennard-Jones Potentials. *J. Phys. Chem. C* **2008**, *112*, 17281–17290. [CrossRef]
61. Mahdavian, L.; Monajjemi, M. Alcohol sensors based on SWNT as chemical sensors: Monte Carlo and Langevin dynamics simulation. *Microelectron. J.* **2010**, *41*, 142–149. [CrossRef]
62. Aihara, J. Reduced HOMO−LUMO Gap as an Index of Kinetic Stability for Polycyclic Aromatic Hydrocarbons. *J. Phys. Chem. A* **1999**, *103*, 7487–7495. [CrossRef]
63. Silverstein, R.M.; Bassler, G.C.; Morrill, T.C. *Spectrometric Identification of Organic Compounds*, 5th ed.; John Wiley & Sons, Inc.: New York, NY, USA, 1981.
64. Zadeh, M.A.A.; Lari, H.; Kharghanian, L.; Balali, E.; Khadivi, R.; Yahyaei, H.; Mollaamin, F.; Monajjemi, M. Density functional theory study and anti-cancer properties of shyshaq plant: In view point of nano biotechnology. *J. Comput. Theor. Nanosci.* **2015**, *12*, 4358–4367. [CrossRef]
65. Khalili Hadad, B.; Mollaamin, F.; Monajjemi, M. Biophysical chemistry of macrocycles for drug delivery: A theoretical study. *Russ. Chem. Bull.* **2011**, *60*, 238–241. [CrossRef]
66. Monajjemi, M.; Lee, V.S.; Khaleghian, M.; Honarparvar, B.; Mollaamin, F. Theoretical Description of Electromagnetic Nonbonded Interactions of Radical, Cationic, and Anionic NH2BHNBHNH2 Inside of the B18N18 Nanoring. *J. Phys. Chem. C* **2010**, *114*, 15315–15330. [CrossRef]
67. Ahmadi, R.; Pishghadam, S.; Mollaamine, F.Z.; Monfared, M.R. Comparing the Effects of Ginger and Glibenclamide on Dihydroxybenzoic Metabolites Produced in Stz-Induced Diabetic Rats. *Int. J. Endocrinol. Metab.* **2013**, *11*, e10266. [CrossRef] [PubMed]
68. Mollaamin, F.; Monajjemi, M. DFT outlook of solvent effect on function of nano bioorganic drugs. *Phys. Chem. Liq.* **2012**, *50*, 596–604. [CrossRef]
69. Khaleghian, M.; Zahmatkesh, M.; Mollaamin, F.; Monajjemi, M. Investigation of Solvent Effects on Armchair Single-Walled Carbon Nanotubes: A QM/MD Study. *Fuller. Nanotub. Carbon Nanostruct.* **2011**, *19*, 251–261. [CrossRef]
70. Lee, V.S.; Nimmanpipug, P.; Mollaamin, F.; Kungwan, N.; Thanasanvorakun, S.; Monajjemi, M. Investigation of single wall carbon nanotubes electrical properties and normal mode analysis: Dielectric effects. *Russ. J. Phys. Chem. A* **2009**, *83*, 2288–2296. [CrossRef]

71. Monajjemi, M.; Ghiasi, R.; Ketabi, S.; Passdar, H.; Mollaamin, F. A Theoretical Study of Metal-Stabilised Rare Tautomers Stability: N4 Metalated Cytosine (M = Be^{2+}, Mg^{2+}, Ca^{2+}, Sr^{2+} and Ba^{2+}) in Gas Phase and Different Solvents. *J. Chem. Res.* **2004**, *2004*, 11–18. [CrossRef]
72. Mollaamin, F.; Varmaghani, Z.; Monajjemi, M. Dielectric effect on thermodynamic properties in vinblastine by DFT/Onsager modelling. *Phys. Chem. Liq.* **2011**, *49*, 318–336. [CrossRef]